Studying the polytropic behavior of an ICME using Multi-spacecraft observation by STEREO-A, STEREO-B, and WIND

Kalpesh Ghag[1], Prachi Pathare[1], Anil Raghav[1,*], Georgios Nicolaou[2], Zubair Shaikh[3], Omkar Dhamane[1], Utsav Panchal[1], Kishor Kumbhar[1], Prathmesh Tari[1], Bhagyashri Sathe[1], Vinit Pawaskar[1], and Greg Hilbert[1]

[1]Department of Physics, University of Mumbai, Mumbai, 400098, India
[2]Department of Space and Climate Physics, Mullard Space Science Laboratory, University College London, Dorking, Surrey, RH5 6NT, UK
[3]Space Sciences Laboratory, University of California, Berkeley, CA 94720, USA
[*]anil.raghav@physics.mu.ac.in

ABSTRACT

The polytropic behavior describes the relationship between macroscopic properties of plasma species and provides useful information in understanding physical mechanisms in space plasma. Through the value of the polytropic index, which governs the polytropic relationship, we can identify the energy transfer in plasma systems. In this paper, we determine the polytropic index of proton plasma within an Interplanetary Coronal Mass Ejection (ICME), which has been observed by three different spacecraft at ~ 1 AU, each separated by $\sim 20^{\circ}$ degrees in longitude during the analyzed observations. By performing this multi-spacecraft analysis, we provide evidence that the polytropic index does not vary significantly across the structure of the observed ICME. This may imply that the ICME evolution process is nearly coherent. Moreover, the polytropic index values we derive here can set boundary conditions in existing and future ICME evolution models.

1 Introduction

Most of the astrophysical and space plasma is in the form of weakly coupled charged particles. The proton thermal pressure $P_{th} = nK_BT$ (K_B is the Boltzmann constant) is similar to that of an ideal gas Livadiotis [38]. Hence, one of the three thermodynamic variables—thermal pressure P_{th}, number density n, and temperature T is always dependent on the other two, such as

$$P_{th} \propto n^{\alpha} \qquad T \propto n^{\alpha-1} \tag{1}$$

where α is known as the polytropic index. Equation 1 indicates the relationship between the variables P, n, and T for quasi-stable and reversible. This process is called polytropic process [10]. It is necessary that the specific heat should remain constant throughout the polytropic process; otherwise, the polytropic index becomes a variable. By taking natural logarithm of Eq. 1, we get

$$\ln P_{th} = \alpha \ln n + \ln F. \tag{2}$$

which shows linear relationship between $\ln P_{th}$ and $\ln n$, while $\ln F$ is a constant (intercept). In data analyses, the polytropic index is often determined from the slope of a linear fitting of Eq. 2 to the scatter plot of $\ln P_{th}$ vs $\ln n$. Therefore, we can determine the polytropic index through the possible correlations between plasma moments and use it to study its thermodynamics. The polytropic index describes the thermodynamic process of a system, e.g., an isothermal process for $\alpha = 1$, an isobaric process for $\alpha = 0$, an isochoric process for $\alpha \longrightarrow \infty$, and so on [42]. In other words, the polytropic index describes the changes in temperature as the system is compressed or expands [58]. Note that in general, the polytropic index α is different from the well-known quantity $\gamma = \frac{c_p}{c_v}$, i.e., the ratio of the specific heats. The value of α=γ is found only in the special case (adiabatic case), in which there is no heat transfer (c= $\frac{dQ}{dT}$ =0). Polytropic indices are routinely used for describing phenomena like the ambient solar wind expansion and the plasma dynamics within planetary magnetospheres, magnetic clouds, and the inner heliosheath [55, 58, 79, 92]. The polytropic index also specifies boundary conditions across discontinuities [37, 57, 74].

Moreover, Akiyama et al. [2] has modeled the first image of a black hole using MHD, which includes the polytropic equation illustrating how plasma modeling is essential to numerous recent high-profile astrophysics discoveries. The polytropic index shows different values in different astrophysical domains, i.e., for galaxy cluster and galaxy supercluster, it has value $\alpha \sim 1.2$ - 1.3 and $\alpha \sim 1.16$ respectively [16, 49]. The polytropic index value of the solar corona is $\alpha = 1.10$ [66, 81]. Houston et al. [24] shows that the polytropic index (α) of the upper chromosphere is 1.12. For hot flare loop the α has value ~ 1.64 [83] and for solar flare it has value $\alpha = 1.64$ - 1.66 [19, 83]. Liu et al. [35] determined α=1.3 by analyzing observations of an ICME plasma within 0.3 and 20 AU. Moreover, the magnetic clouds of ICMEs show variation as $1.1 \leq \alpha \leq 1.3$ [35]. Mishra and Wang [50] modeled an ICME propagating within the heliosphere, revealing that α drops from $\alpha = 1.87$ to $\alpha = 1.3$ as it propagates away from the sun. A similar but systematic drop of the polytropic index during ICMEs was also detected and investigated by Dayeh and Livadiotis [13]. In the region of the solar wind at 1 AU, the proton and electron show $\alpha = 1.46$ - 1.67 and $\alpha = 1$ respectively [41, 56, 80]. In planetary region $\alpha = 1.85$ for bow-shock of Venus and for earth's plasma sheet $\alpha \sim 1.67$ [79, 92].

ICMEs are large-scale magnetic structures containing huge mass, kinetic energy, and magnetic flux that are expelled from the Sun into the interplanetary space [8, 11, 21, 26, 73, 89]. Therefore, ICMEs can significantly disturb the solar wind in the interplanetary space and the near-earth space [9, 31, 36, 72]. They have paramount importance in space weather studies not only for their natural hazardous effects on humans and the technology in space and ground but also for their considerable disruption threat to the global economy which leads to the extensive studies of their macro-structure ([23, 62, 75]).

ICME *in-situ* studies are commonly associated with three main observations: the forward propagating shock, the magnetically connected and organised flux rope, and the turbulent sheath between the shock front and the flux rope [4, 5, 30, 93]. The flux rope, or as often called magnetic cloud (MC), is a loop of twisted magnetic field lines confining a plasma of low proton beta [5, 32]. The magnetic field strength enhancement, large and smooth rotations of the magnetic field components, and low ion temperatures/plasma beta constitute the observational signature of MCs. While not all ICMEs contain magnetic cloud (MC) structures, it's worth noting that certain indicators may still be present in some ICMEs despite the absence of all expected MC characteristics. These ICMEs usually lack typical MC attributes like a consistently rotating IMF and a strengthened magnetic field. Therefore, when ICMEs do not possess all the defining features of an MC, they are referred to as magnetic ejecta [7]. The *in-situ* features of a typical MC/ejecta at 1 AU last for $1-2$ days. The flux ropes / MCs are modeled as cylindrical structures and toroidal configurations. The evidence appears to support the assumption that the ICME foot-legs are rooted to the Sun [27, 33, 52]. However, ICMES can be comprised of open and closed field lines [3].

This study will contribute to our understanding of previously unexplored aspects of plasma physics : (i) the kinematic and thermodynamic evolution of an expanding magnetized plasma blob in an ambient magneto-fluid medium, and (ii) mechanisms for energy exchange and plasma dynamics across distinct plasma regions of the ICME [25, 43, 44]. Osherovich et al. [61] measured different polytropic indices for electrons and protons during the passage of MC. The proton temperature is correlated with the density, and the average polytropic index is 1.2, whereas electrons are anti-correlated, having a polytropic index α = -0.48. The thermodynamic evolution of an ICME from 0.3 to 30 AU has been studied with the help of *in-situ* observations [35, 82]. Liu et al. [35] shows the Coulomb collision within ICMEs and their moderate expansion compared with theoretical predictions. Furthermore, they suggest that the slow decrease in the temperature inside the ICME, compared to the solar wind temperature drop, gives insights into the heating process of the ICME. The polytropic index of CME plasma was estimated statistically to be between 1.1 and 1.3 from 0.3 to 20 AU, with no significant variations over the solar cycle [35]. This suggests that the expansion of ICME is nearly isothermal in nature. However, [41, 55, 80] found empirically the polytropic index of solar wind is near adiabatic. This implies that the ICME plasma is different from the ambient solar wind. Mishra and Wang [50] found that the polytropic index for CME varies from α= 1.87 to α= 1.3 as it propagates away from the sun. These modeling results are quite different from the traditional observations by Liu et al. [35]. Recently, Dayeh and Livadiotis [13] investigated the polytropic index of ICMEs in the four distinct regions, i.e., sheath, MC, pre-and post-ICME region. The pre-and post-ICME regions were found to be near adiabatic. They estimated deviation in the polytropic index from the adiabatic value for the sheath region ($\alpha - \gamma = 0.26$) and the MC ($\alpha - \gamma = 0.13$). They further claimed that the larger deviation leads to a larger entropy gradient. Thus, it implies a higher rate of turbulent heating for the sheath region than the MC of the ICME plasma.

The near adiabatic polytropic process is entropy conserving and thus reversible, whereas the turbulent behavior of plasma may be irreversible [20, 35] while it is connected with a non-adiabatic polytropic index [39, 40]. This is inspiring in using a combination of turbulence theory and polytropic behavior in the thermodynamic modeling of ICME and their observation in interplanetary space. The ambiguity between observations and modeling results may be challenging in future studies of ICME evolution. Moreover, the understanding of the continuous evolution of the thermodynamic state of an individual CME during its heliospheric propagation is still limited. Due to the large dimensions of ICME, systematic multi-point polytropic measurements are necessary to study the radially expanding ICME across different regions. As the ICME expands over time and space, it is possible to examine the evolution of these processes by studying radially aligned spacecraft at various distances in the heliosphere. It is worth noting that studying thermodynamic properties as a function of radial distance from the Sun is a crucial method for comprehending the physical properties and heating processes of ICMEs. As a result, analyzing a collection

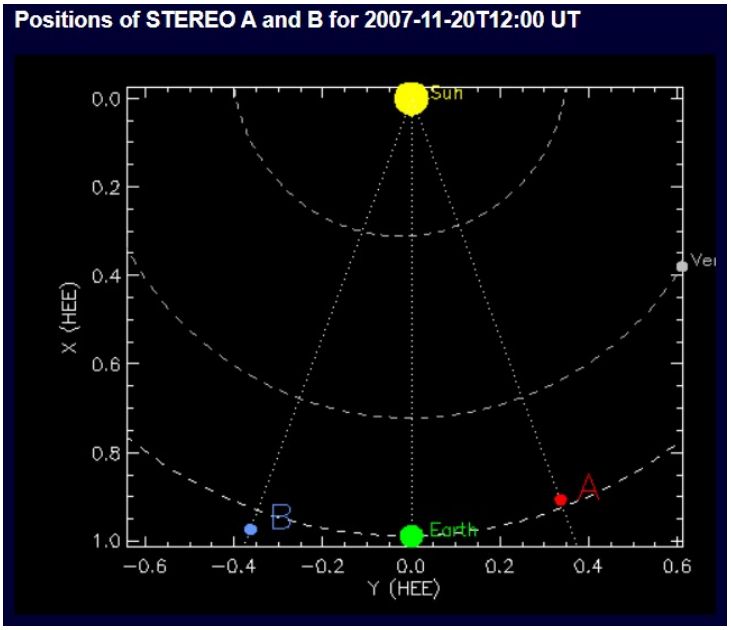

Figure 1. Position of Spacecrafts in Heliocentric Earth-Ecliptic coordinate obtained from https://stereo-ssc.nascom.nasa.gov/where.shtml

of ICMEs is necessary to make informed judgments about the evolution of thermodynamic properties from a single location.

Here we estimate polytropic indices of ICME observed on November 19 -20, 2007, using *in-situ* observations by STEREO-A, STEREO-B, and WIND spacecraft. These multi-spacecraft measurements provide a unique opportunity to examine the thermodynamic behavior of ICME at three different longitudes. The study will clarify whether the information is spreading longitudinally throughout the ICME. It will be essential to comprehend the coherent or incoherent evolution of the ICME.

2 Data and Methods

In this study, we analyze *in-situ* observations obtained by STEREO-A (STA), STEREO-B (STB), and WIND spacecraft. On November 20, 2007, at 12 : 00 UT, the three spacecraft were at 0.97 AU, 1.04 AU, and 0.99 AU from the Sun, respectively. The heliospheric latitude and longitude of the spacecrafts are STA ($-0.38°$, $20.23°$), STB ($4.77°$, $-20.35°$), and WIND ($2.2°$, $0.0°$) as shown in Figure1. STA and STB are separated longitudinally with $40.58°$, which is equivalent to 0.86 AU. This offers a great opportunity to study properties of the same structure from two vastly different locations.

Spacecraft	Locations (in lat. and long.)	Rad. dist. (in AU)	Shock onset	MC start	MC end	Bmag nT	Vp kms-1	Np cm-3	Pth nPa
STA	($-0.38°$, $20.23°$)	0.97		Nov., 19, 23:00	Nov. 20, 23:40	8.99	416.49	7.54	0.0038
WIND	($2.2°$, $0.0°$)	0.99	Nov. 19, 17:22	Nov. 20, 00:20	Nov. 20, 11:40	18.17	464.83	12.85	0.0058
STB	($4.77°$, $-20.35°$)	1.04	Nov. 19, 13:49	Nov. 19, 23:00	Nov. 20, 07:00	13.72	437.26	16.25	0.0160

Table 1. Summary of the analyzed observations by the three spacecrafts.

We analyze 1-min resolution observations of plasma protons obtained by PLASTIC instruments [18, 45] onboard STA and STB. We specifically use the solar wind proton speed V_p, proton number density N_p, and proton temperature T_p. We use 1-min resolution data of the magnetic field components (B_x, B_y, and B_z) obtained by MAG instruments on board the STEREO spacecraft [1, 45]. We also analyze proton plasma parameters (V_p, N_p, and T_p) and B-field components (B_x, B_y and B_z) obtained by the Solar Wind Experiment (SWE, [60]) and magnetic field investigation (MFI, [34]) on board WIND, respectively. These observations by WIND are provided with 92-sec resolution.

We apply a linear fit model to the scatter plot between logarithms of thermal pressure and the logarithm of density (equation 2) for the interested regions to estimate the polytropic index. The fitted line has a slope of α, a polytropic index. If the polytropic index is estimated using linear fits to $\ln T_p$ vs $\ln N_p$, then the slope of the fitted line is $\alpha - 1$ instead of α.

3 Observation

We utilized the ICME identification criteria outlined in earlier studies (See Raghav et al. [67, 68, 69], Raghav and Kule [70], Raghav et al. [71], Richardson and Cane [73], Shaikh et al. [76, 77] and references there in). Furthermore, we cross-checked the ICME boundaries using the WIND and STA/STB catalogs, which can be accessed at at 1) https://wind.nasa.gov/ICME_catalog/ICME_catalog_viewer.php 2) https://stereo-ssc.nascom.nasa.gov/events.shtml

3.1 *In-situ* observation of interplanetary parameters by STEREO-A

The heliocentric distance of STEREO-A was 0.96 AU on 19 November 2007, having separation angle of 20.46° with Earth/ WIND spacecraft. Figure 2 (a) shows the time series of the B-field and plasma parameters for the ICME event, as observed by STA. We did not detect any significant sudden or abrupt increases in the total IMF (B_{mag}), solar wind velocity (V_p), or proton number density (N_p). This suggests that the spacecraft (STA) did not traverse the shock front. Furthermore, the variations in B_{mag} and its components were minimal, and there was no noticeable enhancement in proton density. Based on these observations, we can conclude that STA did not pass through the sheath region of the interplanetary coronal mass ejection (ICME). However, on 19 November 2007, at 22:57 UT, there was a decrease in plasma beta, number density, and IMF rotation, indicating that the spacecraft did cross the magnetic cloud (MC). Inside the MC, there was a gradual increase in the magnetic field strength from 7 nT to 11 nT. We noticed a rise in β on 20 November 2007, at 23:36, which we interpret as the boundary of the magnetic cloud. The total duration of the spacecraft's transit through the MC was 24 hours and 26 minutes.

3.2 *In-situ* observation of interplanetary parameters by WIND

The WIND spacecraft is situated at the L1 point. It is at a heliocentric distance of 0.989 AU on 20 Nov 2007. On 19 November 2007, at 17:22 UT, a forward shock with a high velocity of 438 km/s was detected. This was identified by a sudden increase in solar wind velocity (V_p), indicating the initiation of the shock. Subsequently, high proton number density (N_p) and plasma beta (β) values were observed, along with significant fluctuations in the magnetic field (B) components. These observations suggest the passage through the sheath region. The duration of the spacecraft's transit through the sheath region lasted approximately 6.24 hours, from November 19, 2007, 17:23 UT to November 19, 2007, 23:47 UT. Moreover, a gradual enhancement in the magnitude of the magnetic field (B_{mag}) from 10 nT to 20 nT was observed, accompanied by rotations in the IMF components. Additionally, a decrease in proton number density (N_p), plasma beta (β), and thermal pressure (P_{th}) was noted, indicating the characteristic features of a magnetic cloud (MC). On November 20, 2007, at 11:19 UT, a rise in plasma beta (β) was observed, which we interpret as the trailing boundary of the magnetic cloud (MC). The duration of the spacecraft's transit through the MC was approximately 12 hours and 28 minutes.

3.3 *In-situ* observation of interplanetary parameters by STEREO-B

In Figure 2 (c), we show STB observations obtained from November 19, 2007, to November 20, 2007, when the spacecraft was at 1.03 AU and had a separation angle of 20.40° with Earth / WIND spacecraft. The spacecraft encountered the shock front at 13:49 UT on November 19, 2007, as evidenced by a sudden and significant increase in magnetic field magnitude (B_{mag}), solar wind velocity (V_p), and proton number density (N_p). The spacecraft remained within the sheath region, which is the region downstream of the shock, until 22:52 UT on November 19, 2007. The sheath region was characterized by high fluctuations in B_{mag} and its components, along with elevated values of N_p, V_p, and plasma beta (β). Notably, during this event, STB observed the sheath region for approximately 9 hours, which is the longest sheath interval recorded in this particular event. From 19 November 2007, 22:52 UT, to 20 November 2007, 14:38 UT, we observed an enhanced magnetic field and rotations in the IMF components. Concurrently, there was a gradual decrease in V_p, low values of N_p and β, indicating the passage through a magnetic cloud (MC). On 20 November 2007, at 14:38 UT, an increase in plasma beta (β) was observed, which we interpret as the boundary of the magnetic cloud (MC). Remarkably, this particular MC interval lasted for 8 hours and 34 minutes, representing the shortest duration among the three spacecraft studied in this event.

3.4 Polytropic Analysis

In Figure 2 (d), (e), and (f), we show $\ln P_{th}$ vs $\ln N_p$ for the MC observations by STA, WIND, and STB, respectively. Linear fits of the data points determine the polytropic index of MC at the observation location. Our analysis determines $\alpha = 1.2$ at the STA location and $\alpha = 1.3$ at STB and WIND locations.

4 Discussions and Conclusion

The multipoint examination of an ICME event is essential to understand the global evolution of magnetic structure and shape of ICMEs in the heliosphere [53]. Here, we study the multi-spacecraft observations of an earthward propagating ICME. The orbiting trajectories of STA, WIND, and STB provide the properties of ICME along its longitudinal spread.

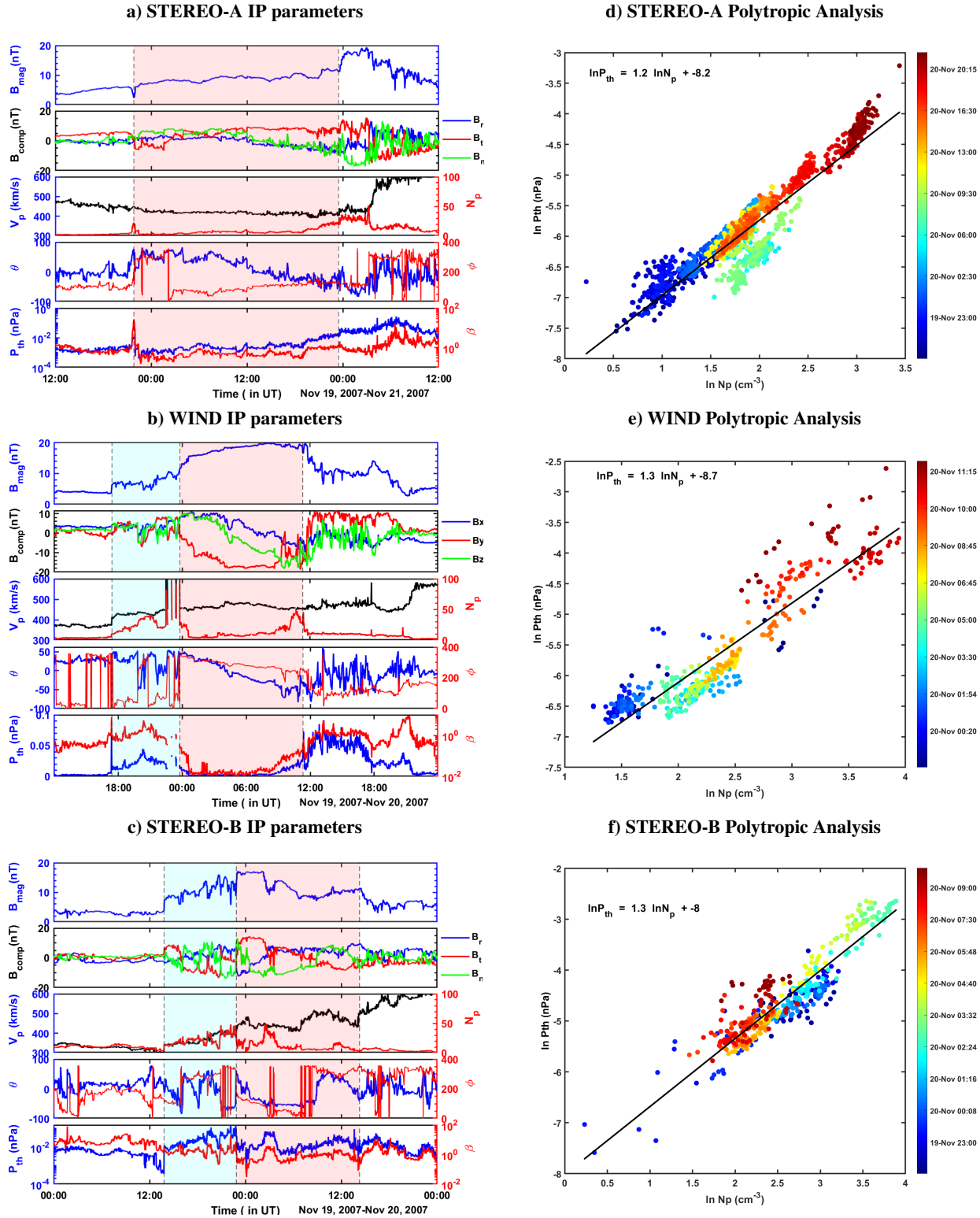

Time series of B-field and plasma parameters as observed by (a) STA, (b) WIND, and (c) STB during the ICME event on November 20, 2007. From top panel shows the i) total magnetic field B_{mag} ii) Magnetic field components (B_x, B_y, B_z) iii) proton velocity(V_p) and proton number density (N_p), iv) The inclination angle of magnetic field vector (θ) and azimuth angle (ϕ) v) thermal pressure (P_{th}) and plasma beta (β). For figures (a), (b), and (c), the cyan-shaded region shows sheath, and the red-shaded region shows magnetic cloud. $\ln P_{th}$ vs $\ln N_p$ from MC observations by (d) STA, (e) WIND, and (f) STB. The solid line in each plot is the linear fitting of equation 2 to the observations, which determines the polytropic index

The magnetic field within an MC is different from the ambient interplanetary (solar wind) field. We routinely observe strongly helical magnetic fields within MCs. Thus the plasma behavior and energy transport inside MC is expected to differ from the solar wind. The MC resembles a flux rope-like structure which may expand, deform, kink-rotate, and deflect during the propagation [12, 28, 29, 35, 47, 48, 84, 85, 86, 87, 88]. Note that the ICMEs expand slightly faster than the spherically diverging flow of the surrounding solar wind. The flux ropes erupting from the Sun have high internal magnetic pressures. Thus, the departures from force-free equilibrium are common in ICMEs, providing an overpressure condition that can drive expansion [35]. Moreover, CMEs have a nearly constant (Sun-centred) angular size while the transverse size increases linearly with distance from the Sun [22, 78, 90]. The ICME expansion is often observed *in situ* as plasma structures with decreasing speed and number density [17]. Thus, we can expect a faster decrease in the temperature of ICMEs than ambient solar wind due to the expansion of ICME's termed as adiabatic cooling [35].

Several studies have used the polytropic processes approach to investigate the thermodynamics of ICME structures. Osherovich et al. [61] estimates the average polytropic index as 1.2 at 1 AU, whereas Liu et al. [35] shows that the polytropic index of ICME is 1.1 $\sim$ 1.3. This implies that the expansion of ICMEs is between sub-adiabatic and near-isothermal, meaning that there is heat flowing to the system that increases the temperature against the adiabatic cooling during expansion. Interestingly, Mishra and Wang [50] and Mishra et al. [51] argue that ICME structures have an adiabatic behavior in the vicinity of the corona, from where they are ejected. Therefore, it is possible that ICMEs evolve from nearly adiabatic structures at the corona to quasi-isothermal plasma structures at $\sim$ 1 AU. Moreover, Liu et al. [35] finds an isothermal plasma within an ICME at $\sim$ 20 AU. So, there is a possibility that ICMEs maintain their isothermal behavior as they propagate beyond 1 AU. In this study, we found polytropic index value 1.2, 1.2, and 1.3 at STA, STB and Wind respectively at three different crossover of ICME. These values are consistent with the previously reported measurements [35, 61]. It is thus interesting to investigate mechanisms that trigger the appropriate heat transfer between ICMEs and the surrounding plasma and fields, which result in this behaviour.

The ICME is a massive magnetic structure with approximately 0.2 AU radial dimension at 1 AU [54]. The electron pitch-angle distributions obtained within ICMEs, reveal bi-directional beams, which implies that the ICME's foot legs are connected at Sun [15, 46, 91]. Various flux-rope models based on *in-situ* observations assumed that the MC has coherent structures [6, 14, 65]. Numerical simulation studies also assumed ICMEs as purely hydrodynamic structures with small-scale coherence across its non-radial direction [59, 64]. Owens et al. [63] claimed that most of the time, the geometric expansion speed of an expanding ICME exceeds its local Alfvén speed. It implies that the information cannot propagate across ICMEs, and they are unable to behave as coherent, solid-like structures even if the magnetic curvature forces would be sufficient in magnitude to resist the external deformation forces [63]. It is very important to know whether the ICME has a coherent or incoherent structure to advance our understanding of the evolution and propagation of ICMEs and their interaction with the surrounding solar wind plasma. In this study, we use observations from 3 different spacecraft and found a similar thermodynamic behavior across an ICME structure. This could be a result of ICMEs being coherent structures, after all. However, we do not neglect the possibility that the ICME we study here has not undergone any significant interaction that would trigger a non-uniform thermodynamic behaviour.

In summary, we suggest that the polytropic method is a macroscopic approach to examine the ICME properties such as ICME expansion and heat exchange, coherence in ICME, etc. Our results suggest that the ICME properties remain unaltered along its longitudinal spread. The three spacecraft have a separation of 20° in longitude at 1 *AU* distance from the Sun. Although 20° may seem like a small window at the observational point of around 1 *AU*, it is significant for studying the plasma properties in the magnetic cloud (MC). Within this window, the plasma characteristics in the MC exhibit similar thermodynamic behaviors, albeit with slight polytropic variations. The fitting result indicates α value of 1.2 for the STA location and α value of 1.3 at the STB location, which has an approximate longitude difference of 40°. Thus we conclude that in the limit of small angle difference 20° longitude, the polytropic index value of ICME evolution/expansion has a coherent nature. This might help validate the coherent behavior of ICME during its propagation. Understanding whether an ICME is coherent or not is crucial because it has a significant impact on the disturbances that occur in near-earth space. The coherency of an ICME is a critical factor to consider when using MHD modelling to simulate its evolution in interplanetary space. Furthermore, this property is crucial in studying how ICMEs interact with the earth's magnetosphere, which is essential for predicting space weather disturbances caused by ICMEs. In fact, studying the coherency of ICMEs can help improve our modelling of ICME-driven space weather disturbances, ultimately enhancing our ability to predict space weather.

Acknowledgements

We acknowledge the use of NASA/GSFC's Space Physics Data Facility's CDAWeb service. The data are publicly available at (1) NASA's Goddard Space Flight Center (GSFC) https://wind.nasa.gov/data.php, and (2) Coordinated Data Analysis Web (CDAWeb) https://cdaweb.gsfc.nasa.gov/pub/data/wind/ We thank DST, India since KG is funded by DST-INSPIRE Fellowship (INSPIRE Fellow Registration Number: IF210212). We acknowledge SERB, India since AR and OD are supported by SERB project reference file number CRG/2020/002314.

References

1. Acuña, M., Curtis, D., Scheifele, J., Russell, C., Schroeder, P., Szabo, A., and Luhmann, J. (2008). The stereo/impact magnetic field experiment. *Space Science Reviews*, 136(1):203–226.

2. Akiyama, K., Alberdi, A., Alef, W., Asada, K., Azulay, R., Baczko, A.-K., Ball, D., Baloković, M., Barrett, J., Bintley, D., et al. (2019). First m87 event horizon telescope results. v. physical origin of the asymmetric ring. *The Astrophysical Journal Letters*, 875(1):L5.

3. Bothmer, V., Desai, M., Marsden, R., Sanderson, T., Trattner, K., Wenzel, K.-P., Gosling, J., Balogh, A., Forsyth, R., and Goldstein, B. (1996). Ulysses observations of open and closed magnetic field lines within a coronal mass ejection. *Astronomy and Astrophysics, v. 316, p. 493-498*, 316:493–498.

4. Bothmer, V. and Schwenn, R. (1997). The structure and origin of magnetic clouds in the solar wind. In *Annales Geophysicae*, volume 16, pages 1–24. Springer.

5. Burlaga, L. (1988). Magnetic clouds and force-free fields with constant alpha. *Journal of Geophysical Research: Space Physics*, 93(A7):7217–7224.

6. Burlaga, L., Fitzenreiter, R., Lepping, R., Ogilvie, K., Szabo, A., Lazarus, A., Steinberg, J., Gloeckler, G., Howard, R., Michels, D., et al. (1998). A magnetic cloud containing prominence material: January 1997. *Journal of Geophysical Research: Space Physics*, 103(A1):277–285.

7. Burlaga, L. F. (1991). Magnetic clouds. In *Physics of the inner heliosphere II: particles, waves and turbulence*, pages 1–22. Springer.

8. Cane, H. and Richardson, I. (2003). Interplanetary coronal mass ejections in the near-earth solar wind during 1996–2002. *Journal of Geophysical Research: Space Physics*, 108(A4).

9. Cargill, P. J. (2004). On the aerodynamic drag force acting on interplanetary coronal mass ejections. *Solar Physics*, 221(1):135–149.

10. Chandrasekhar, S. and Chandrasekhar, S. (1957). *An introduction to the study of stellar structure*, volume 2. Courier Corporation.

11. Chen, P. (2011). Coronal mass ejections: models and their observational basis. *Living Reviews in Solar Physics*, 8(1):1–92.

12. Dasso, S., Mandrini, C. H., Démoulin, P., and Luoni, M. L. (2006). A new model-independent method to compute magnetic helicity in magnetic clouds. *Astronomy & Astrophysics*, 455(1):349–359.

13. Dayeh, M. A. and Livadiotis, G. (2022). Polytropic behavior in the structures of interplanetary coronal mass ejections. *The Astrophysical Journal Letters*, 941(2):L26.

14. Démoulin, P. and Dasso, S. (2009). Magnetic cloud models with bent and oblate cross-section boundaries. *Astronomy & Astrophysics*, 507(2):969–980.

15. Dresing, N., Gómez-Herrero, R., Heber, B., Hidalgo, M. A., Klassen, A., Temmer, M., and Veronig, A. (2016). Injection of solar energetic particles into both loop legs of a magnetic cloud. *Astronomy & Astrophysics*, 586:A55.

16. Ettori, S., Bardelli, S., De Grandi, S., Molendi, S., Zamorani, G., and Zucca, E. (2000). Bepposax-rosat pspc observations of the shapley supercluster: A3562. *Monthly Notices of the Royal Astronomical Society*, 318(1):239–249.

17. Farrugia, C. J., Burlaga, L., Osherovich, V., Richardson, I., Freeman, M., Lepping, R., and Lazarus, A. (1993). A study of an expanding interplanetary magnetic cloud and its interaction with the earth's magnetosphere: The interplanetary aspect. *Journal of Geophysical Research: Space Physics*, 98(A5):7621–7632.

18. Galvin, A. B., Kistler, L. M., Popecki, M. A., Farrugia, C. J., Simunac, K. D., Ellis, L., Möbius, E., Lee, M. A., Boehm, M., Carroll, J., et al. (2008). The plasma and suprathermal ion composition (plastic) investigation on the stereo observatories. *Space Science Reviews*, 136(1):437–486.

19. Garcia, H. (2001). Polytropic indices of solar flares. *ApJ*, 557(2):897–905.

20. Goldstein, M. L., Roberts, D. A., and Matthaeus, W. (1995). Magnetohydrodynamic turbulence in the solar wind. *Annual review of astronomy and astrophysics*, 33:283–326.

21. Gopalswamy, N., Mäkelä, P., Xie, H., Akiyama, S., and Yashiro, S. (2009a). Cme interactions with coronal holes and their interplanetary consequences. *Journal of Geophysical Research: Space Physics*, 114(A3).

22. Gopalswamy, N., Yashiro, S., Michalek, G., Stenborg, G., Vourlidas, A., Freeland, S., and Howard, R. (2009b). The soho/lasco cme catalog. *Earth, Moon, and Planets*, 104(1):295–313.

23. Hapgood, M. (2012). Prepare for the coming space weather storm. *Nature*, 484(7394):311–313.

24. Houston, S., Jess, D., Ramos, A. A., Grant, S., Beck, C., Norton, A., and Prasad, S. K. (2018). The magnetic response of the solar atmosphere to umbral flashes. *ApJ*, 860(1):28.

25. Howard, T., Fry, C., Johnston, J., and Webb, D. (2007). On the evolution of coronal mass ejections in the interplanetary medium. *The Astrophysical Journal*, 667(1):610.

26. Hundhausen, A. J., Sawyer, C. B., House, L., Illing, R., and Wagner, W. (1984). Coronal mass ejections observed during the solar maximum mission: Latitude distribution and rate of occurrence. *Journal of Geophysical Research: Space Physics*, 89(A5):2639–2646.

27. Kahler, S. and Reames, D. (1991). Probing the magnetic topologies of magnetic clouds by means of solar energetic particles. *Journal of Geophysical Research: Space Physics*, 96(A6):9419–9424.

28. Kay, C., Opher, M., and Evans, R. (2015). Global trends of cme deflections based on cme and solar parameters. *The Astrophysical Journal*, 805(2):168.

29. Kay, C., Opher, M., and Evans, R. M. (2013). Forecasting a coronal mass ejection's altered trajectory: Forecat. *The Astrophysical Journal*, 775(1):5.

30. Kilpua, E., Jian, L., Li, Y., Luhmann, J., and Russell, C. (2012). Observations of icmes and icme-like solar wind structures from 2007–2010 using near-earth and stereo observations. *Solar Physics*, 281(1):391–409.

31. Kilpua, E., Koskinen, H. E., and Pulkkinen, T. I. (2017). Coronal mass ejections and their sheath regions in interplanetary space. *Living Reviews in Solar Physics*, 14(1):1–83.

32. Klein, L. and Burlaga, L. (1982). Interplanetary magnetic clouds at 1 au. *Journal of Geophysical Research: Space Physics*, 87(A2):613–624.

33. Larson, D., Lin, R., McTiernan, J., McFadden, J., Ergun, R., McCarthy, M., Reme, H., Sanderson, T., Kaiser, M., Lepping, R., et al. (1997). Tracing the topology of the october 18–20, 1995, magnetic cloud with $0.1–10^2$ kev electrons. *Geophysical research letters*, 24(15):1911–1914.

34. Lepping, R., Acũna, M., Burlaga, L., Farrell, W., Slavin, J., Schatten, K., Mariani, F., Ness, N., Neubauer, F., Whang, Y., et al. (1995). The wind magnetic field investigation. *Space Science Reviews*, 71(1-4):207–229.

35. Liu, Y., Richardson, J., Belcher, J., Kasper, J., and Elliott, H. (2006). Thermodynamic structure of collision-dominated expanding plasma: Heating of interplanetary coronal mass ejections. *Journal of Geophysical Research: Space Physics*, 111(A1).

36. Liu, Y. D., Luhmann, J. G., Kajdič, P., Kilpua, E. K., Lugaz, N., Nitta, N. V., Möstl, C., Lavraud, B., Bale, S. D., Farrugia, C. J., et al. (2014). Observations of an extreme storm in interplanetary space caused by successive coronal mass ejections. *Nature Communications*, 5(1):1–8.

37. Livadiotis, G. (2015). Shock strength in space and astrophysical plasmas. *The Astrophysical Journal*, 809(2):111.

38. Livadiotis, G. (2016). Superposition of polytropes in the inner heliosheath. *The Astrophysical Journal Supplement Series*, 223(1):13.

39. Livadiotis, G. (2019). Connection of turbulence with polytropic index in the solar wind proton plasma. *Entropy*, 21(11):1041.

40. Livadiotis, G. (2021). Radial profile of the polytropic index of solar wind plasma in the heliosphere. *Research Notes of the AAS*, 5(1):4.

41. Livadiotis, G. and Desai, M. I. (2016). PLASMA-FIELD COUPLING AT SMALL LENGTH SCALES IN SOLAR WIND NEAR 1 au. *ApJ*, 829(2):88.

42. Livadiotis, G. and McComas, D. (2012). Non-equilibrium thermodynamic processes: Space plasmas and the inner heliosheath. *The Astrophysical Journal*, 749(1):11.

43. Lopez, R. E., Goodrich, C., Wiltberger, M., and Lyon, J. (2000). Solar wind–magnetosphere energy coupling under extreme interplanetary conditions: Mhd simulations. *Journal of Atmospheric and Solar-Terrestrial Physics*, 62(10):865–874.

44. Low, B. (2001). Coronal mass ejections, magnetic flux ropes, and solar magnetism. *Journal of Geophysical Research: Space Physics*, 106(A11):25141–25163.

45. Luhmann, J., Curtis, D., Schroeder, P., McCauley, J., Lin, R., Larson, D., Bale, S., Sauvaud, J.-A., Aoustin, C., Mewaldt, R., et al. (2008). Stereo impact investigation goals, measurements, and data products overview. In *The STEREO Mission*, pages 117–184. Springer.

46. Malandraki, O., Sarris, E., Lanzerotti, L., Trochoutsos, P., Tsiropoula, G., and Pick, M. (2002). Solar energetic particles inside a coronal mass ejection event observed with the ace spacecraft. *Journal of atmospheric and solar-terrestrial physics*, 64(5-6):517–525.

47. Manchester IV, W., Gombosi, T., De Zeeuw, D., Sokolov, I., Roussev, I., Powell, K., Kóta, J., Tóth, G., and Zurbuchen, T. (2005). Coronal mass ejection shock and sheath structures relevant to particle acceleration. *The Astrophysical Journal*, 622(2):1225.

48. Manchester IV, W. B., Gombosi, T. I., Roussev, I., Ridley, A., De Zeeuw, D. L., Sokolov, I., Powell, K. G., and Tóth, G. (2004). Modeling a space weather event from the sun to the earth: Cme generation and interplanetary propagation. *Journal of Geophysical Research: Space Physics*, 109(A2).

49. Markevitch, M., Forman, W. R., Sarazin, C. L., and Vikhlinin, A. (1998). The temperature structure of 30 nearby clusters observed with asca: Similarity of temperature profiles. *The Astrophysical Journal*, 503(1):77.

50. Mishra, W. and Wang, Y. (2018). Modeling the thermodynamic evolution of coronal mass ejections using their kinematics. *ApJ*, 865(1):50.

51. Mishra, W., Wang, Y., Teriaca, L., Zhang, J., and Chi, Y. (2020). Probing the thermodynamic state of a coronal mass ejection (cme) up to 1 au. *Frontiers in Astronomy and Space Sciences*, 7:1.

52. Möstl, C., Farrugia, C. J., Temmer, M., Miklenic, C., Veronig, A. M., Galvin, A. B., Leitner, M., and Biernat, H. K. (2009). Linking remote imagery of a coronal mass ejection to its in situ signatures at 1 au. *The Astrophysical Journal*, 705(2):L180.

53. Möstl, C., Weiss, A. J., Reiss, M. A., Amerstorfer, T., Bailey, R. L., Hinterreiter, J., Bauer, M., Barnes, D., Davies, J. A., Harrison, R. A., et al. (2022). Multipoint interplanetary coronal mass ejections observed with solar orbiter, bepicolombo, parker solar probe, wind, and stereo-a. *The Astrophysical Journal Letters*, 924(1):L6.

54. Mulligan, T. and Russell, C. (2001). Multispacecraft modeling of the flux rope structure of interplanetary coronal mass ejections: Cylindrically symmetric versus nonsymmetric topologies. *Journal of Geophysical Research: Space Physics*, 106(A6):10581–10596.

55. Newbury, J., Russell, C., and Lindsay, G. (1997a). Solar wind polytropic index in the vicinity of stream interactions. *GRL*, 24(11):1431–1434.

56. Newbury, J. A., Russell, C. T., and Lindsay, G. M. (1997b). Solar wind polytropic index in the vicinity of stream interactions. *GRL*, 24(11):1431–1434.

57. Nicolaou, G. and Livadiotis, G. (2017). Modeling the plasma flow in the inner heliosheath with a spatially varying compression ratio. *The Astrophysical Journal*, 838(1):7.

58. Nicolaou, G., Livadiotis, G., and Moussas, X. (2014). Long-term variability of the polytropic index of solar wind protons at 1 au. *Solar Physics*, 289(4):1371–1378.

59. Odstrcil, D., Riley, P., and Zhao, X. (2004). Numerical simulation of the 12 may 1997 interplanetary cme event. *Journal of Geophysical Research: Space Physics*, 109(A2).

60. Ogilvie, K., Chornay, D., Fritzenreiter, R., Hunsaker, F., Keller, J., Lobell, J., Miller, G., Scudder, J., Sittler, E., Torbert, R., et al. (1995). Swe, a comprehensive plasma instrument for the wind spacecraft. *Space Science Reviews*, 71(1):55–77.

61. Osherovich, V., Farrugia, C., Burlaga, L., Lepping, R., Fainberg, J., and Stone, R. (1993). Polytropic relationship in interplanetary magnetic clouds. *JGR: Space Physics*, 98(A9):15331–15342.

62. Oughton, E., Copic, J., Skelton, A., Kesaite, V., Yeo, Z., Ruffle, S. J., and Ralph, D. (2016). Helios solar storm scenario. *Cambridge Risk Framework series*.

63. Owens, M., Lockwood, M., and Barnard, L. (2017). Coronal mass ejections are not coherent magnetohydrodynamic structures. *Scientific Reports*, 7(1):1–6.

64. Owens, M. J. (2020). Coherence of coronal mass ejections in near-earth space. *Solar Physics*, 295(10):1–13.

65. Owens, M. J., Merkin, V., and Riley, P. (2006). A kinematically distorted flux rope model for magnetic clouds. *Journal of Geophysical Research: Space Physics*, 111(A3).

66. Prasad, S. K., Raes, J., Van Doorsselaere, T., Magyar, N., and Jess, D. (2018). The polytropic index of solar coronal plasma in sunspot fan loops and its temperature dependence. *ApJ*, 868(2):149.

67. Raghav, A., Gaikwad, S., Wang, Y., Shaikh, Z. I., Mishra, W., and Zao, A. (2020). Study of flux-rope characteristics at sub-astronomical-unit distances using the helios 1 and 2 spacecraft. *Monthly Notices of the Royal Astronomical Society*, 495(2):1566–1576.

68. Raghav, A., Shaikh, Z., Vemareddy, P., Bhaskar, A., Dhamane, O., Ghag, K., Tari, P., Dayanandan, B., and Mohammed Al Suti, B. (2023). The possible cause of most intense geomagnetic superstorm of the 21st century on 20 november 2003. *Solar Physics*, 298(5):64.

69. Raghav, A. N., Choraghe, K., and Shaikh, Z. I. (2019). The cause of an extended recovery from an icme-induced extreme geomagnetic storm: a case study. *MNRAS*, 488(1):910–917.

70. Raghav, A. N. and Kule, A. (2018). The first in situ observation of torsional alfvén waves during the interaction of large-scale magnetic clouds. *MNRAS: Letters*, 476(1):L6–L9.

71. Raghav, A. N., Kule, A., Bhaskar, A., Mishra, W., Vichare, G., and Surve, S. (2018). Torsional alfvén wave embedded icme magnetic cloud and corresponding geomagnetic storm. *ApJ*, 860(1):26.

72. Richardson, I. and Cane, H. (2011). Geoeffectiveness (dst and kp) of interplanetary coronal mass ejections during 1995–2009 and implications for storm forecasting. *Space Weather*, 9(7).

73. Richardson, I. G. and Cane, H. V. (2010). Near-earth interplanetary coronal mass ejections during solar cycle 23 (1996–2009): Catalog and summary of properties. *Solar Physics*, 264(1):189–237.

74. Scherer, K., Fichtner, H., Fahr, H. J., Röken, C., and Kleimann, J. (2016). Generalized multi-polytropic rankine–hugoniot relations and the entropy condition. *The Astrophysical Journal*, 833(1):38.

75. Schrijver, C. J., Kauristie, K., Aylward, A. D., Denardini, C. M., Gibson, S. E., Glover, A., Gopalswamy, N., Grande, M., Hapgood, M., Heynderickx, D., et al. (2015). Understanding space weather to shield society: A global road map for 2015–2025 commissioned by cospar and ilws. *Advances in Space Research*, 55(12):2745–2807.

76. Shaikh, Z., Raghav, A., and Vichare, G. (2022). Comparative statistical plasma properties of planar and non-planar icme during solar cycles 23 and 24. *44th COSPAR Scientific Assembly. Held 16-24 July*, 44:1541.

77. Shaikh, Z. I., Raghav, A., and Vichare, G. (2019). Coexistence of a planar magnetic structure and an alfvén wave in the shock-sheath of an interplanetary coronal mass ejection. *MNRAS*, 490(2):1638–1643.

78. Siscoe, G. and Odstrcil, D. (2008). Ways in which icme sheaths differ from magnetosheaths. *Journal of Geophysical Research: Space Physics*, 113(A9).

79. Tatrallyay, M., Russell, C. T., Luhmann, J. G., Barnes, A., and Mihalov, J. D. (1984). On the proper mach number and ratio of specific heats for modeling the venus bow shock. *JGR: Space Physics*, 89(A9):7381–7392.

80. Totten, T., Freeman, J., and Arya, S. (1995). An empirical determination of the polytropic index for the free-streaming solar wind using helios 1 data. *JGR: Space Physics*, 100(A1):13–17.

81. Van Doorsselaere, T., Wardle, N., Del Zanna, G., Jansari, K., VERwICHTE, E., and NAkARIAkOV, V. M. (2011). The first measurement of the adiabatic index in the solar corona using time-dependent spectroscopy of hinode/eis observations. *ApJL*, 727(2):L32.

82. Wang, C., Du, D., and Richardson, J. (2005). Characteristics of the interplanetary coronal mass ejections in the heliosphere between 0.3 and 5.4 au. *Journal of Geophysical Research: Space Physics*, 110(A10).

83. Wang, T., Ofman, L., Sun, X., Provornikova, E., and Davila, J. M. (2015). Evidence of thermal conduction suppression in a solar flaring loop by coronal seismology of slow-mode waves. *ApJL*, 811(1):L13.

84. Wang, Y., Shen, C., Liu, R., Liu, J., Guo, J., Li, X., Xu, M., Hu, Q., and Zhang, T. (2018). Understanding the twist distribution inside magnetic flux ropes by anatomizing an interplanetary magnetic cloud. *Journal of Geophysical Research: Space Physics*, 123(5):3238–3261.

85. Wang, Y., Shen, C., Wang, S., and Ye, P. (2004). Deflection of coronal mass ejection in the interplanetary medium. *Solar Physics*, 222(2):329–343.

86. Wang, Y., Wang, B., Shen, C., Shen, F., and Lugaz, N. (2014). Deflected propagation of a coronal mass ejection from the corona to interplanetary space. *Journal of Geophysical Research: Space Physics*, 119(7):5117–5132.

87. Wang, Y., Xue, X., Shen, C., Ye, P., Wang, S., and Zhang, J. (2006). Impact of major coronal mass ejections on geospace during 2005 september 7-13. *The Astrophysical Journal*, 646(1):625.

88. Wang, Y., Zhang, Q., Liu, J., Shen, C., Shen, F., Yang, Z., Zic, T., Vrsnak, B., Webb, D., Liu, R., et al. (2016). On the propagation of a geoeffective coronal mass ejection during 15–17 march 2015. *Journal of Geophysical Research: Space Physics*, 121(8):7423–7434.

89. Wimmer-Schweingruber, R., Crooker, N., Balogh, A., Bothmer, V., Forsyth, R., Gazis, P., Gosling, J., Horbury, T., Kilchenmann, A., Richardson, I., et al. (2006). Understanding interplanetary coronal mass ejection signatures. *Coronal Mass Ejections*, pages 177–216.

90. Yashiro, S., Gopalswamy, N., Michalek, G., St. Cyr, O., Plunkett, S., Rich, N., and Howard, R. (2004). A catalog of white light coronal mass ejections observed by the soho spacecraft. *Journal of Geophysical Research: Space Physics*, 109(A7).

91. Zharkova, V. and Xia, Q. (2021). Pitch-angle distribution of accelerated electrons in 3d current sheets with magnetic islands. *Astronomy & Astrophysics*, 648:A51.

92. Zhu, X. (1990). Plasma sheet polytropic index as inferred from the fpe measurements. *GRL*, 17(13):2321–2324.

93. Zurbuchen, T. H. and Richardson, I. G. (2006). In-situ solar wind and magnetic field signatures of interplanetary coronal mass ejections. *Coronal mass ejections*, pages 31–43.